

# Learning Deep Matrix Representations

**Kien Do**

**Truyen Tran**

**Svetha Venkatesh**

*Applied AI Institute, Deakin University, Australia*

DKDO@DEAKIN.EDU.AU

TRUYEN.TRAN@DEAKIN.EDU.AU

SVETHA.VENKATESH@DEAKIN.EDU.AU

**Editors:** XXX

## Abstract

We present a new distributed representation in deep neural nets wherein the information is represented in native form as a matrix. This differs from current neural architectures that rely on vector representations. We consider matrices as central to the architecture and they compose the input, hidden and output layers. The model representation is more compact and elegant – the number of parameters grows only with the largest dimension of the incoming layer rather than the number of hidden units. We derive several new deep networks: (i) feed-forward nets that map an input matrix into an output matrix, (ii) recurrent nets which map a sequence of input matrices into a sequence of output matrices. We also reinterpret existing models for (iii) memory-augmented networks and (iv) graphs using matrix notations. For graphs we demonstrate how the new notations lead to simple but effective extensions with multiple attentions. Extensive experiments on handwritten digits recognition, face reconstruction, sequence to sequence learning, EEG classification, and graph-based node classification demonstrate the efficacy and compactness of the matrix architectures.

## 1. Introduction

Recent advances in deep learning have generated a constant stream of new neural architectures, including skip-connections to differentiable external memories (LeCun et al., 2015; Graves et al., 2016; Greff et al., 2017). The canonical representation of information in these architectures still remains the vector form since the backprop (Rumerhart et al., 1986):

$$\mathbf{y} = \sigma(W\mathbf{x} + \mathbf{b}) \quad (1)$$

where  $\mathbf{x}, \mathbf{y}$  are vector representation of neuron activation;  $W, b$  are parameters and  $\sigma$  is a non-linear transformation.

While vector representation has enjoyed a great popularity, it is unstructured and hence unnaturally for many settings in which structures are essential. When a data instance is two-way and associative, Eq. (1) necessitates vectorization of data matrices, leading to a very large mapping weight matrix  $W$  and a loss of structure in the representation by vector  $\mathbf{x}$ . Examples of two-way data include time-channel recording as in EEG signals, disease progression in medical records, and n-gram of word embeddings. Examples of associative data (or bipartite graphs) include interaction matrix of two object classes (e.g., style/context and content), player-club affiliation, member-task assignments, and covariance matrices (Huang and Van Gool, 2017). In those cases, it is more natural to directly use matrix representation of data (Gao et al., 2017; Nguyen et al., 2015).

Moreover, matrix representation of hidden neurons is an efficient way to hold more information and enable powerful attention mechanisms (Bahdanau et al., 2015). For example, a bidirectional

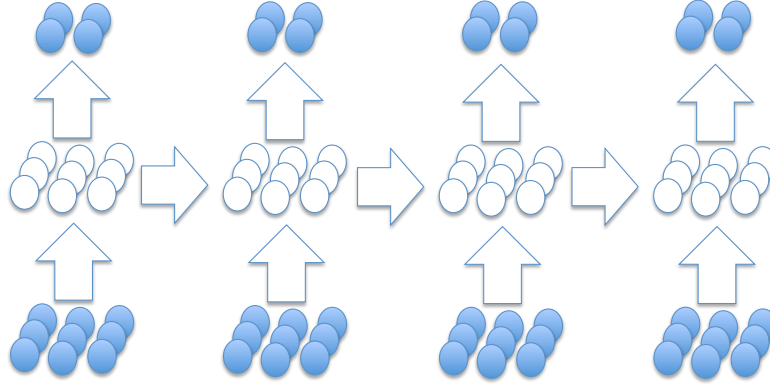


Figure 1: Matrix recurrent neural nets. Circles represent neurons, arrows represent the directions of influence.

LSTM sitting on top of a sentence produce a set of state vectors, one per word. These vectors naturally form a matrix; and in translation, attention to specific row of the matrix has proved to be essential to state-of-the-art results (Bahdanau et al., 2015). Importantly, the state matrix plays the role of a matrix memory with column memory slots in memory-augmented recurrent nets (Weston et al., 2014; Graves et al., 2014; Santoro et al., 2016).

In this paper, we formalize those separate ideas by deriving *a new common building block of neuron networks in that all the neuron representations are matrices*. We replace Eq. (1) by the following:

$$Y = \sigma(U^\top X V + B) \quad (2)$$

where  $X, Y$  are matrix representation;  $U, V, B$  are parameters. While this idea has been suggested in a contemporary work of (Gao et al., 2017), our work aims to be more thorough and systematic. First, we generalize state-of-the-art feed-forward neural networks and recurrent neural networks (RNNs) to accommodate matrix forms (see Fig. 1 for an illustration of a matrix RNN). Second, we demonstrate how to formulate recent memory-augmented networks using the matrix representation with appropriate choice of weights  $U$  and  $V$  in Eq. (2). Third, we show that several recent neural graph models are actually instances of matrix nets, and how matrix representation leads to expressive extensions to include multiple attentions.

Moreover, to prove the advantages of this new representation, we have designed a comprehensive suite of five different experiments. In the first two, we explore the learning curves of matrix feed-forward nets and the reconstruction capability of matrix auto-encoders to support an argument that the matrix mapping in Eq. (2) does provide a so-called “*structural regularization*” which cannot be seen on the vector mapping. In the next two, we test the performance of matrix recurrent nets on 2 tasks: sequence-to-sequence learning and classification of EEG signals. Our purpose is to assert that matrix recurrent nets with more memory but far fewer parameters can easily outperform the vector counterparts. In the last experiment, we demonstrate matrix-based graph models on node classification for citation networks, showing how matrix representation improves upon vector representation, and how matrix gives rise to multi-attention mechanisms that offers further improvement.

## 2. Matrix Networks

We design matrix-based neural networks where the input, output, hidden state and memory are matrices. Let us start by introducing some notations:

$$\text{mat}_1(P; \theta_1) := U^\top PV + B \quad (3)$$

where  $P \in \mathbb{R}^{r \times c}$  is a neuron matrix of  $r$  rows and  $c$  columns,  $U \in \mathbb{R}^{r \times r'}$  and  $V \in \mathbb{R}^{c \times c'}$  are called *row-mapping* and *column-mapping* matrices respectively,  $B \in \mathbb{R}^{r' \times c'}$  is a bias matrix and  $\theta_1 = \{U, V, B\}$  denotes parameters of the model.

Next, we will show how to derive (i) multi-attention mechanisms (Sec. 2.1) (ii) new matrix-based deep feed-forward nets (Sec. 2.2), and (iii) new matrix recurrent nets (Sec. 2.3).

### 2.1. Multi-Attention and Memory

In Eq. (3), given a matrix  $P$  of  $r$  rows, we can soft-attend to its rows by requiring  $U = [\alpha_1, \alpha_2 \dots \alpha_k]$ , where each  $\alpha_j$  is an attention vector subject to  $\sum_{i=1}^m \alpha_{ij} = 1$  and  $\alpha_{ij} \geq 0$  for  $j = 1, 2, \dots, k$ . In this setting, each read pass returns an aggregated vector:

$$s_j = \alpha_j^\top P \quad (4)$$

which is then transformed using the transformation matrix  $V$ . Typically,  $\alpha_j$  is parameterized using a neural network with softmax activation, possibly as a function of  $P$  and its context (if available).

Indeed, several memory-augmented networks such as Neural Turing Machine (Graves et al., 2014), Memory Network (Weston et al., 2014), End-to-End Memory Network (Sukhbaatar et al., 2015) can be formulated in similar ways with  $P$  being the external memory and  $U$  is the collection of read heads.

### 2.2. Matrix Feed-forward Nets

The one-layer matrix feed-forward net that maps a matrix input  $X$  onto a matrix output  $Y$  (*mat2mat*) is readily defined as:

$$Y = \sigma_Y(\text{mat}_1(X; \theta_Y)) \quad (5)$$

Deep models can be generalized as usual by stacking multiple hidden matrix layers. To improve the fast credit assignment for very deep nets, we can employ *skip-connections*, just like the case of vector-based nets. In vector representation, it typically takes the following form:

$$\mathbf{h}_t = \mathbf{r}_t \odot \mathbf{h}_{t-1} + \mathbf{z}_t \odot \tilde{\mathbf{h}}_t$$

where  $\mathbf{h}_t$  and  $\tilde{\mathbf{h}}_t$  are the final and intermediate representation at step  $t$  (assuming  $\mathbf{h}_0$  is the input vector  $\mathbf{x}$ ),  $\mathbf{r}_t \in [0, 1]$ ,  $\mathbf{z}_t \in [0, 1]$  are gates, and  $\odot$  is point-wise multiplication. The layer  $t-1$  is said to be skip-connected<sup>1</sup> to layer  $t$  through the term  $\mathbf{r}_t \odot \mathbf{h}_{t-1}$ . The extension to matrix is straightforward:

$$H_t = R_t \odot H_{t-1} + Z_t \odot \tilde{H}_t$$

---

1. The skip-connections can indeed go further down many times and many steps to  $t-k$ , for  $k = 1, 2, \dots, t-1$ , e.g., see (Huang et al., 2017).

For example, the Highway Network (Srivastava et al., 2015b) can be extended as:

$$\begin{aligned} Z_t &= \text{sigm}(\text{mat}_1(H_{t-1}; \theta_{t,z})) \\ \tilde{H}_t &= \sigma(\text{mat}_1(H_{t-1}; \theta_{t,h})) \\ H_t &= (1 - Z_t) \odot H_{t-1} + Z_t \odot \tilde{H}_t \end{aligned}$$

Here  $R_t = 1 - Z_t$ . The matrix ResNet (He et al., 2016) is similar:  $H_t = H_{t-1} + F(H_t)$  where  $F(H_t)$  is a residual feedforward subnet that map a matrix  $H_t$  into another matrix  $\tilde{H}_t$  in the same space. These networks can be made recurrent by typing parameters across layers.

### 2.3. Matrix Recurrent Nets

The standard vector-based recurrent neural network is a mapping from a vector sequence to another sequence. The matrix alternative thus maps an input matrix sequence  $X_{1:T}$  to an output matrix sequence  $Y_{1:T}$ , via a hidden matrix sequence  $H_{1:T}$ , as follows. Let:

$$\text{mat}_2(P, Q; \theta_2) := U_p^\top P V_p + U_q^\top Q V_q + B \quad (6)$$

where  $P, Q$  are neuron matrices and  $\theta_2 = \{U_p, V_p, U_q, V_q, B\}$  are parameters. The network dynamics are summarized in the following equations:

$$Y_t = \sigma_Y(\text{mat}_1(H_t; \theta_Y)) \quad (7)$$

$$H_t = \sigma_H(\text{mat}_2(X_t, H_{t-1}; \theta_H)) \quad (8)$$

The number of parameters is roughly quadratic in the dimensions of matrices  $X_t, H_t, Y_t$ . This is inline with the capacity of the short-term memory stored in  $H_t$ . Thus the parameter–memory ratio is a constant, unlike the ratio in the classical case of vector memory, which grows linearly with vector size.

The generalization from vanilla matrix RNN to matrix LSTM is straightforward. The formula of a LSTM block (without peep-hole connection) at time step  $t$  can be specified as follows:

$$\begin{aligned} I_t &= \text{sigm}(\text{mat}_2(X_t, H_{t-1}; \theta_i)) \\ F_t &= \text{sigm}(\text{mat}_2(X_t, H_{t-1}; \theta_f)) \\ O_t &= \text{sigm}(\text{mat}_2(X_t, H_{t-1}; \theta_o)) \\ \hat{C}_t &= \tanh(\text{mat}_2(X_t, H_{t-1}; \theta_c)) \\ C_t &= F_t \odot C_{t-1} + I_t \odot \hat{C}_t \\ H_t &= O_t \odot \tanh(C_t) \end{aligned}$$

where  $\odot$  denotes the Hadamard product; and  $I_t, F_t, O_t, \hat{C}_t$  are input gate, forget gate, output gate and cell gate at time  $t$ , respectively. Note that the memory cells  $C_t$  that store, forget and update information is a matrix.

To save space for other discussion, we will not present the formula of the matrix GRU here since it can easily be derived from the formulas of vector GRU in the same way as LSTM.

### 3. Matrix Representation of Graphs

In this section, we show *how natural the matrix formulation is for deep graph modeling*. In particular, we focus our attention on the work in (Scarselli et al., 2009; Li et al., 2016; Pham et al., 2017). We will use the notation from (Pham et al., 2017), where the network is called Column Network (CLN). For the generalization to other types of graph neural networks (Defferrard et al., 2016; Kipf and Welling, 2016) based on spectral graph theory, please refer to Appx. B.

Let  $\mathcal{G} = (\mathcal{V}, \mathcal{E})$  be a graph, where  $\mathcal{V}$  is a set of nodes and  $\mathcal{E}$  is a set of edges. In CLN, each node in  $\mathcal{V}$  is modeled using a deep feed-forward net such as Highway Network (Srivastava et al., 2015b). Different from standard feed-forward nets, here all nets are inter-connected where information is passed between nets along the edges defined by  $\mathcal{E}$ .

Denote by  $\mathbf{h}_i^t \in \mathbb{R}^{1 \times d}$  the activation vector of node  $i$  at step  $t$ . CLN computes  $\tilde{\mathbf{h}}_i^t$ , an aggregate of neighbor states at step  $t$ , where the neighborhood is defined by  $\mathcal{E}$ :

$$\tilde{\mathbf{h}}_i^t = \frac{1}{|\mathcal{N}(i)|} \sum_{j \in \mathcal{N}(i)} \mathbf{h}_j^t \quad (9)$$

where  $\mathcal{N}(i)$  is the neighborhood of node  $i$ , as defined by  $\mathcal{E}$ . Then the activation is a function of the previous step as follows:

$$\mathbf{h}_i^t = f(\mathbf{h}_i^{t-1}, \tilde{\mathbf{h}}_i^{t-1}) \quad (10)$$

We now show how CLN can be represented using matrix notation. First, all hidden states in step  $t$  can be stacked vertically (by row) to form a matrix  $H^t = [\mathbf{h}_1^t | \mathbf{h}_2^t | \dots | \mathbf{h}_{|\mathcal{V}|}^t]$ , i.e.,  $H^t \in \mathbb{R}^{|\mathcal{V}| \times d}$ . Likewise, let  $\tilde{H}^t = [\tilde{\mathbf{h}}_1^t | \tilde{\mathbf{h}}_2^t | \dots | \tilde{\mathbf{h}}_{|\mathcal{V}|}^t]$ .

Now let  $A$  be the adjacency matrix of graph  $G$  and  $\tilde{A}$  be the normalized version of  $A$ , that is  $\tilde{A}_{ij} = \frac{1}{|\mathcal{N}(i)|}$  for  $j \in \mathcal{N}(i)$  and  $\tilde{A}_{ij} = 0$  for  $j \notin \mathcal{N}(i)$ . Eq. (9) can be written as:

$$\tilde{H}^t = \tilde{A}H^t \quad (11)$$

and Eq. (10) can be rewritten as:

$$H^t = F(H^{t-1}, \tilde{H}^{t-1}) \quad (12)$$

where  $F$  is an arbitrary matrix neural network.

#### 3.1. Column Networks with Multi-Attentions

Putting Eq. (11) in the context of Sec. 2.1 immediately suggests that  $\Lambda$  can be extended to stimulate *attention mechanism* rather than simple averaging. The normalized adjacency matrix  $\tilde{A}$  now becomes the attention matrix  $\Lambda$  whose element  $\Lambda_{ij} > 0$  is the probability that that node  $i$  chooses to include information from node  $j$ .

In our experiment in Sec. 4.4, we use the following attention formula:

$$\Lambda_{ij} = \text{softmax } g(\mathbf{h}_i^{t-1}, \mathbf{h}_j^{t-1})$$

with  $g$  is a bilinear neural network:  $g(\mathbf{x}, \mathbf{y}) = \mathbf{x}^\top W \mathbf{y} + \mathbf{a}^\top \mathbf{x} + \mathbf{b}^\top \mathbf{y} + c$ . The appear of parameter  $W$  in  $g$  allow the interaction between a node  $i$  and its neighbor  $j$  to be captured.

Sometimes, it is not enough to aggregate all neighboring states of a node  $i$  into a single vector, especially when the size of  $\mathcal{N}(i)$  is big (e.g. in a citation network, one paper can be cited by hundreds or thousands of other papers). Therefore, we propose an architecture called “*multi-attention*” where we compute  $n$  attention matrices  $\Lambda^{(1)}, \dots, \Lambda^{(n)}$  using  $n$  different neural networks  $g^{(1)}, \dots, g^{(n)}$ . Replace  $\tilde{A}$  in Eq. (11) by  $\Lambda^{(i)}$  ( $i = \overline{1, n}$ ), we have:

$$\tilde{H}^{(i)t} = \Lambda^{(i)} H^t \quad \forall i = \overline{1, n} \quad (13)$$

and the final  $\tilde{H}^t \in \mathbb{R}^{|\mathcal{V}| \times nd}$  is the concatenation of  $\tilde{H}^{(i)t}$  ( $i = \overline{1, n}$ ) by columns:

$$\tilde{H}^t = \left[ \tilde{H}^{(1)t}, \tilde{H}^{(2)t}, \dots, \tilde{H}^{(n)t} \right]$$

Since  $\tilde{H}^t$  still has matrix form (only its shape is modified), the generic formula in Eq. (12) remains unchanged.

## 4. Experimental Results

In this section, we present experimental results on validating the matrix neural architectures described in Section 2. Our primary purpose is to demonstrate that when matrix-like structures are present, matrix nets will clearly outperform the vector nets. For all experiments presented below, our networks use ReLU activation function and are trained using Adam (Kingma and Ba, 2014) (with default settings).

### 4.1. Learning Characteristics of Matrix Neural Networks

We first evaluate the learning curves for deep matrix feed-forward nets (FFNs) under various settings. For convenience, we use handwritten digit and facial images and treat an image as a matrix, ignoring its translation- and rotation-invariant nature. With these in mind, images can be either row- or column-permuted before feeding to matrix nets, and these rule out applying standard CNN for feature extraction.

#### 4.1.1. MNIST

The MNIST dataset consists of 70K handwritten digits of size  $28 \times 28$ , with 50K images for training, 10K for testing and 10K for validation. To test the ability to accommodate very deep nets without skip-connections (Srivastava et al., 2015b), we create vector and matrix FFNs with increasing depths. The top layers are softmax as usual for both vector and matrix nets. We compare matrix nets with the hidden shape of  $20 \times 20$  and  $50 \times 50$  against vector nets containing 50, 100 and 200 hidden units.

We observe that without Batch-Norm (BN) (Ioffe and Szegedy, 2015), vector nets struggle to learn when the depth goes beyond 20, as expected. The erratic learning curves of the vector nets at depth 30 are shown in Fig. 2(a), top row. With the help of BN layers, the vector nets can learn normally at depth 30, but again fail beyond depth 50 (see Fig. 2(a), bottom row). The matrix nets are far better: They learn smoothly at depth 30 without BN layers (Fig. 2(b), top). With BN layers, they

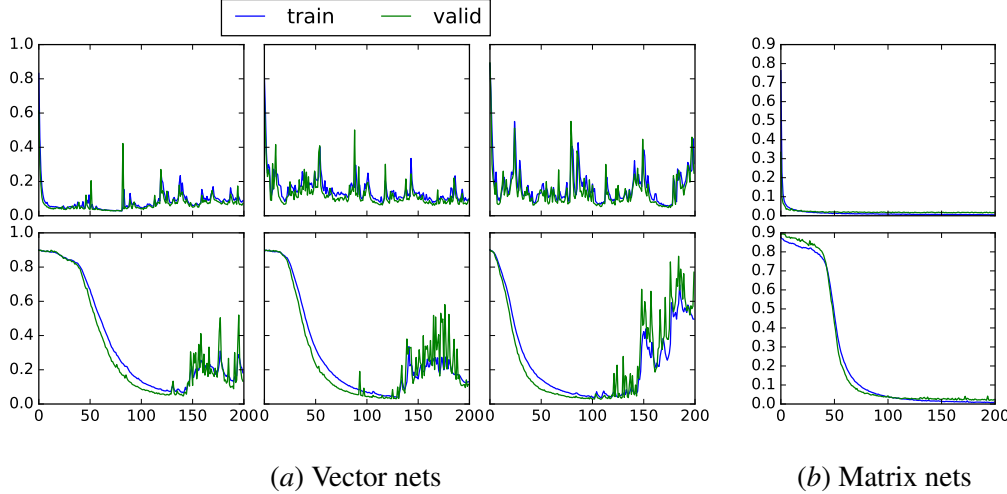


Figure 2: Learning curves of vector and matrix feed-forward nets over MNIST. **(a) Left to right:** Vector nets with 50, 100, 200 hidden units. **(b):** Matrix nets with  $50 \times 50$  hidden units. **Top:** 30-layer nets without Batch Norm. **Bottom:** 50-layer nets with Batch Norm.

still learn well at depth 50 (Fig. 2(b), bottom) and can manage to learn up to depth 70 (result is not shown here).

We visualize the weights of the first layer of the matrix net with hidden layers of  $50 \times 50$  (the weights for  $20 \times 20$  layers are similar) in Fig. 3 for a better understanding. In the plots of  $U$  and  $V$  (top and bottom left of Fig. 3, respectively), the short vertical brushes indicate that some adjacent input features are highly correlated along the row or column axes. For example, the digit 1 has white pixels along its line which will be captured by  $U$ . In case of  $W$ , each square tile in Fig. 3(right) corresponds to the weights that map the entire input matrix to a particular element of the output matrix. These weights have cross-line patterns, which differ from stroke-like patterns commonly seen in vector nets.

#### 4.1.2. MATRIX AUTOENCODERS FOR CORRUPTED FACE RECONSTRUCTION

To evaluate the ability of learning structural information in images of matrix neural nets, we conduct experiments on the Frey Face dataset<sup>2</sup>, which consists of 1,965 face images of size  $28 \times 20$ , taken from sequential frames of a video. We randomly select 70% data for training, 20% for testing and 10% for validation. Test images are corrupted with  $5 \times 5$  black square patches at random positions. Auto-encoders (AEs) are used for this reconstruction task. We build deep AEs consisting of 20 and 40 layers. For each depth, we select vector nets with 50, 100, 200 and 500 hidden units and matrix nets with hidden shape of  $20 \times 20$ ,  $50 \times 50$ ,  $100 \times 100$  and  $150 \times 150$ . The encoders and the decoders have tied weights. The AEs are trained with backprop, random noise added to the input with ratio of 0.2, and L1 and L2 regularizers.

Once trained, AEs are used to reconstruct the test images. Fig. 4 presents several reconstruction results. Vector AEs fail to learn to reconstruct either with or without weight regularization. Without

2. <http://www.cs.nyu.edu/~roweis/data.html>

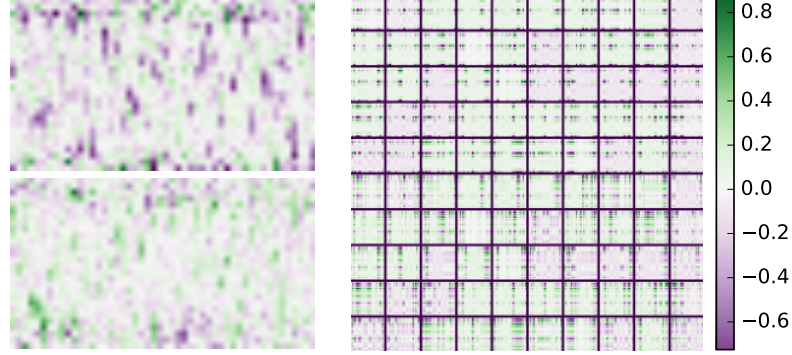


Figure 3: The normalized weights of the first layer of the 30-layer matrix feed-forward net with hidden size of  $50 \times 50$  trained on MNIST. Weights of other layers look quite similar. **Top left:** Row mapping matrix  $U$  of shape  $28 \times 50$ . **Bottom left:** Column mapping matrix  $V$  of shape  $28 \times 50$ . **Right:** Each square tile  $i, j$  show the weight  $W_{:,i \times 50+j}$  which is the outer product of  $U_{:,i}$  and  $V_{:,j}$ .

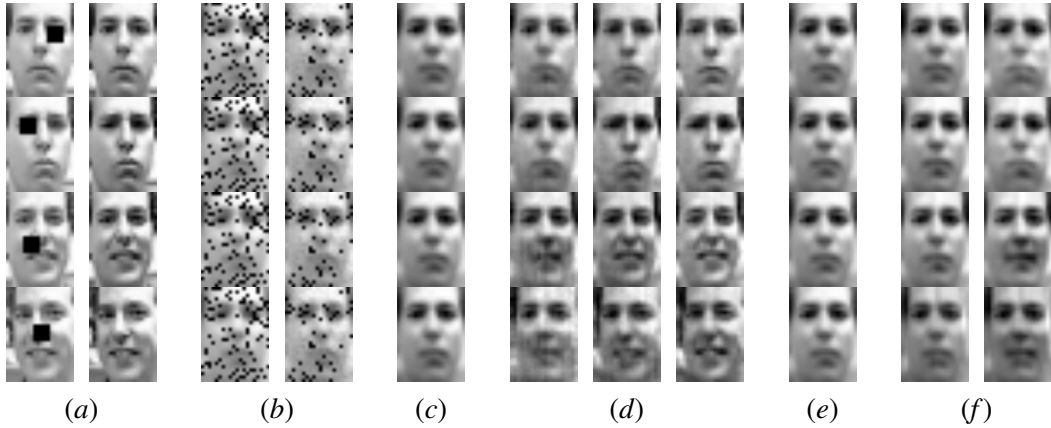


Figure 4: Images reconstructed by matrix AEs and vector AEs in comparison with ground truth. All AEs from **(b)** to **(e)** have 40 layers while the AEs at **(f)** have 20 layers. **(a):** corrupted inputs and ground truth; **(b):** vector AEs (hidden size of 50 and 500) without regularization; **(c):** vector AEs with regularization; **(d):** matrix AEs (hidden size of  $20 \times 20$ ,  $50 \times 50$  and  $150 \times 150$ ) without regularization; **(e):** matrix AEs with L1 regularization; **(f):** matrix AEs (hidden size of  $50 \times 50$  and  $150 \times 150$ ) with L2 regularization.

weight regularization, vector AEs fail to remove noise from the training images (Fig. 4(b)), while with weight regularization they collapse to a single mode (Fig. 4(b))<sup>3</sup>. Matrix AEs, in contrast, can reconstruct the test images quite well *without weight regularization* (see Fig. 4(d)). In fact, adding weight regularization to matrix AEs actually deteriorates the performance, as shown in Figs. 4(e,f).

3. This happens for all hidden sizes and all depth values of vector AEs specified above.

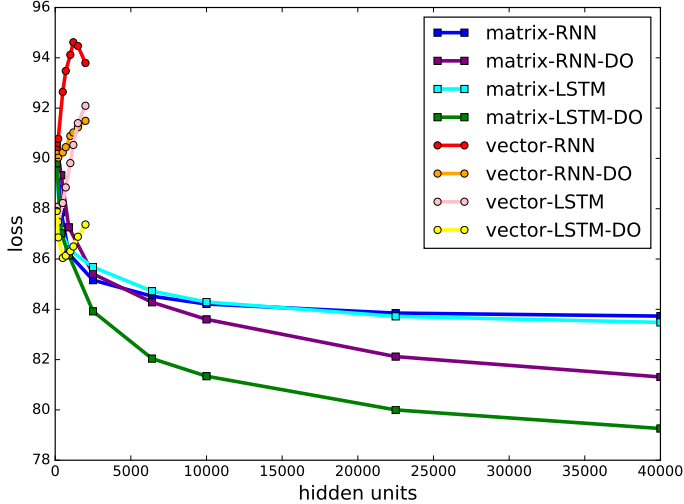


Figure 5: Reconstruction loss over test data of matrix and vector seq2seq models as functions of hidden unit. *DO* is short for Dropout which is set at 0.2 for inputs and 0.5 for hidden units. Best viewed in color.

This suggests an expected behavior in which matrix-like structures in images are preserved in matrix neural nets, enabling missing information to be recovered.

#### 4.2. Sequence to Sequence Learning with Moving MNIST

In this experiment, we compare the performance of matrix and vector recurrent nets in a *sequence-to-sequence* (seq2seq) learning task (Sutskever et al., 2014; Srivastava et al., 2015a). We choose the Moving MNIST dataset<sup>4</sup> which contains 10K image sequences. Each sequence has length of 20 showing 2 digits moving in  $64 \times 64$  frames. We randomly divide the dataset into 6K, 3K and 1K image sequences with respect to training, testing and validation. In our seq2seq model, the encoder and the decoder are both recurrent nets. The encoder captures information of the first 15 frames while the decoder predicts the last 5 frames using the hidden context learnt by the encoder. Different from (Srivastava et al., 2015a), the decoder do not have readout connections<sup>5</sup> for simplicity. We build vector seq2seq models with hidden sizes ranging from 100 to 2000 for both the encoder and the decoder. In case of matrix seq2seq models, we choose hidden sizes from from  $10 \times 10$  to  $200 \times 200$ . Later in this section, we write vector RNN/LSTM to refer to a vector seq2seq model with the encoder and decoder are RNNs/LSTMs. The same notation applies to matrix.

It is important to emphasize that matrix nets are far more compact than the vector counterparts. For example, the vector RNNs require nearly 30M parameters for 2K hidden units while the matrix RNNs only need about 400K parameters (roughly 75 times fewer) but have 40K hidden units (20 times larger)<sup>6</sup>. The parameter inflation exhibits a huge redundancy in vector representation which

4. [http://www.cs.toronto.edu/~nitish/unsupervised\\_video/](http://www.cs.toronto.edu/~nitish/unsupervised_video/)

5. the predicted output of the decoder at one time step will be used as input at the next time step

6. For LSTMs, the number of parameters quadruples but the relative compactness between vector and matrix nets remain the same.

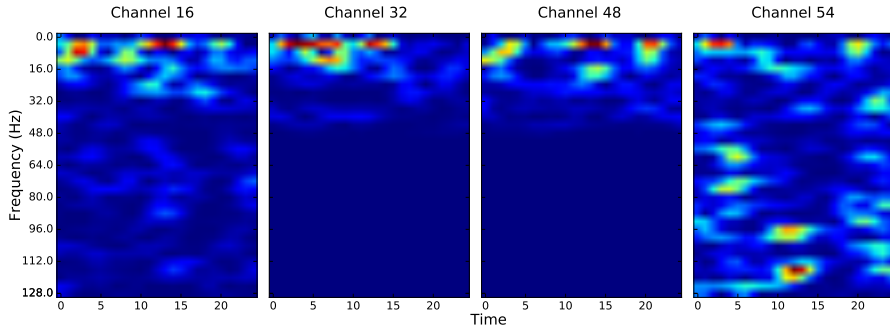


Figure 6: Spectrograms of four channels taken from one trial of a random alcoholic subject. Best viewed in color.

makes the vector nets susceptible to overfitting. Therefore, after a certain threshold (200 in this case), increasing the hidden size of a vector RNN/LSTM will deteriorate its performance. Matrix nets, in contrast, are consistently better when the hidden shape becomes larger, suggesting that overfitting is not a problem. Remarkably, a matrix RNN/LSTM with hidden shape of  $50 \times 50$  is enough to outperform vector RNNs/LSTMs of any size with or without dropout (see Fig. 5). Dropout does improve the representations of both vector and matrix nets but it cannot eliminate the overfitting on the big vector nets.

### 4.3. Sequence Classification with EEG

We use the Alcoholic EEG dataset<sup>7</sup> of 122 subjects divided into two groups: alcoholic and control groups. Each subject completed about 100 trials and the data contains about 12K trials in total. For each trial, the subject was presented with three different types of stimuli in 1 second. EEG signals have 64 channels sampled at the rate of 256 Hz. Thus, each trial consists of  $64 \times 256$  samples in total. We convert the signals into spectrograms using Short-Time Fourier Transform (STFT) with Hamming window of length 64 and 56 overlapping samples. The signals were detrended by removing mean values along the time axis. Because the signals are real-valued, we only take half of the frequency bins. We also exclude the first bin which corresponds to zero frequency. This results in a tensor of shape  $64 \times 32 \times 25$  where the dimensions are channel, frequency and time, respectively. Fig. 6 shows examples of the input spectrogram of an alcoholic subject in 4 channels which reveals some spatial correlations across channels and frequencies. For this dataset, we randomly separate the trials of each subject with a proportion of 0.6/0.2/0.2 for training/testing/validation.

To model the frequency change of all channels over time, we use LSTMs (Hochreiter and Schmidhuber, 1997). We choose vector LSTMs with 200 hidden units which show to work best in the experiment with Moving MNIST. For matrix LSTMs, we select the one with hidden shape of  $100 \times 100$ . Inputs to LSTMs are plain spectrogram which are sequences of matrices of shape  $64 \times 32$ . For vector LSTM, these matrices are flattened into vectors.

As seen in Tab. 1, the vector LSTM with raw input (Model 1) not only achieves the worse result but also consumes a very large number of parameters. The matrix LSTM (Model 2) improves the

7. <https://kdd.ics.uci.edu/databases/eeg/eeg.data.html>

Dataset	#Classes	#Nodes	#Edges	#Features	Node Degree		
					Max	Min	Avg
Citeseer	6	3,312	4,732	3,703	99	1	2.78
Cora	7	2,708	5,429	1,433	168	1	3.90
PubMed	3	19,717	44,338	500	171	1	4.50

Table 2: Statistics of citation network datasets.

result by a large margin (67.7% relative error reduction) while having an order of magnitude fewer parameters than of Model 1.

Model	# Params	Err (%)
vec-LSTM	1,844,201	5.29
mat-LSTM	<b>160,601</b>	<b>1.71</b>

Table 1: Results on EEG classification.

#### 4.4. Multi-Attention Matrix for Graph Modeling

From existing work (Kipf and Welling, 2016), we select 3 large citation network datasets: Citeseer, Cora and PubMed, whose statistics are reported in Tab. 2. In each dataset, nodes are publications and (undirected) edges are citation links between those publications. Each node is represented as a bag-of-words feature vector and is assigned with a label indicating the type of the publication. The task is node classification. Similar to (Kipf and Welling, 2016), we randomly select 1000 nodes for testing and leave the remaining for training/validation. The number of nodes for validation is set to 1000 for PubMed and 100 for Cora and Citeseer.

Our models used in this experiment are derived from the Column Networks (CLN) (Pham et al., 2017). We implemented three variants. The default variant uses mean pooling to aggregate information from neighbors, as in Eq. (9). For the other two variants, vector CLN simply flattens the matrix of neighbors into vector and multi-attention CLN applies multi-attention mechanism presented in Sec. 3.1.

Our settings are similar for all three models: 50 for the number of neighbors per node (randomly sampled during training), 100 for the number of hidden units in case of the PubMed dataset and 20 for the other 2 datasets, 5 for the height of the column networks (the range within which a node can receive messages from its neighbors) and  $5 \times 10^{-4}$  for L2 regularization. Besides, the number of attention is set to 10 in case of multi-attention CLN. Its means that our attention matrix will have the shape  $10 \times 50$ . We train the models using 100 epochs. Early stopping is triggered if the validation loss does not improve after 10 consecutive epochs. The best test results of each model from 10 different runs are reported in Tab. 3.

Model	Citeseer	Cora	PubMed
vector CLN	70.2%	79.2%	88.8%
CLN	72.3%	81.4%	89.1%
multi-attention CLN	<b>72.6%</b>	<b>81.7%</b>	<b>89.7%</b>

Table 3: Results of node classification on citation networks.

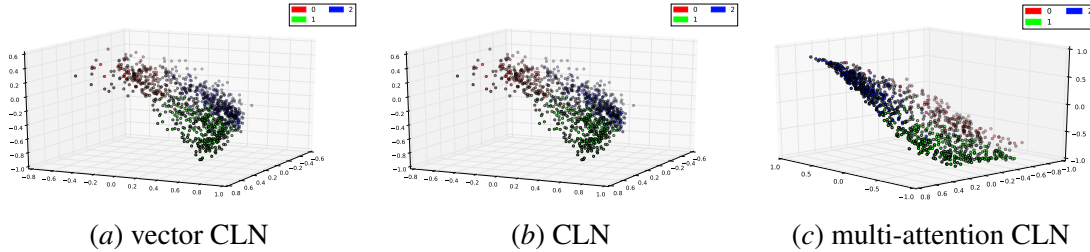


Figure 7: t-SNE visualization of the last hidden states in three variants of CLN. Best viewed in color

Under the same settings, vector CLN achieves the worst results in all three datasets. It suggests that vectorizing the neighbor matrix is not a good strategy in graph modeling, especially when the graph is sparse, since most of the weights are wasteful. Meanwhile, aggregation methods like the default CLN and multi-attention CLN can easily avoid this problem and provide better results. We also observed that multi-attention CLN slightly outperforms the default CLN. Our intuition is that multi-attention CLN allows a node to accumulate more information. We also provide the 3D t-SNE (van der Maaten and Hinton, 2008) visualization of the last hidden representations of all model on the test PubMed dataset for further understanding. Interestingly, they exhibit 3 distinct patterns. For the vector CLN, the points seem to contract around a line while for the default CLN, they lie on a nearly perfect plane (although we embed them on 3D). In case of the multi-attention CLN, we, instead, observe a curved surface. We think this should be investigated more in the future work.

## 5. Related Work

Matrix data modeling has been well studied in shallow or linear settings, such as 2DPCA (Yang et al., 2004), 2DLDA (Ye et al., 2004), Matrix-variate Factor Analysis (Xie et al., 2008), Tensor RBM (Nguyen et al., 2015; Qi et al., 2016). Except 2DPCA and 2DLDA, all other methods are probabilistic models which use matrix mapping to parameterize the conditional distribution of the observed random variable given the latent variable. However, since these models are shallow, their applications of matrix mapping are limited.

Deep learning inspired models for handling multidimensional data including Multidimensional RNNs (Graves and Schmidhuber, 2009), Grid LSTMs (Kalchbrenner et al., 2015) and Convolutional LSTMs (Xingjian et al., 2015). The main idea of the Multidimensional RNNs and Grid LSTMs is that any spatial dimension can be considered as a temporal dimension. They extend the standard recurrent networks by making as many new recurrent connections as the dimensionality of the data. These connections allow the network to create a flexible internal representation of the surrounding context. Although Multidimensional RNNs and Grid LSTMs are shown to work well with many high dimensional datasets, they are complicate to implement and have a very long recurrent loop (often equal to the input tensor’s shape) run sequentially. A convolutional LSTM, on the other hand, works like a standard recurrent net except that its gates, memory cells and hidden states are all 3D tensors with convolution as the mapping operator. Consequently, each local region in the hidden memory is attended and updated over time. However, not like our matrix neural nets, applying convolutional LSTM to memories and graphs is not straightforward.

There has been a large amount of work on graph modeling recently. Apart from those (Perozzi et al., 2014; Grover and Leskovec, 2016) based on skip-gram model (Mikolov et al., 2013) to learn node representations (by using random walk to find node neighborhoods), other methods explicitly exploit the graph structure (via its adjacency matrix) to exchange states between nodes. Although they originate from different viewpoints, e.g. spectral graph theory (Defferrard et al., 2016; Kipf and Welling, 2016) and message propagation (Scarselli et al., 2009; Li et al., 2016; Pham et al., 2017), their formulations (with some restrictions like no edge types) are, indeed, special cases of our matrix neural nets (see Sec. 3 and the Appx. B).

## 6. Discussion

This study investigated an alternative distributed representation in neural nets where information is distributed across neurons arranged in a matrix. This departs from the existing canonical representation using vectors. Comprehensive experimental results have demonstrated that our matrix models perform significantly better than the vector counterparts when data are inherently matrices. Besides, matrix representation is naturally in line with recent memory-augmented RNNs and graph neural networks. This suggest a new way of thinking and opens a wide room for future work.

## Appendix A. Matrix GRU

Likewise, the GRU block is specified as:

$$\begin{aligned} Z_t &= \text{sigm}(\text{mat}_2(X_t, H_{t-1}; \theta_z)) \\ R_t &= \text{sigm}(\text{mat}_2(X_t, H_{t-1}; \theta_r)) \\ \tilde{H}_t &= \sigma(\text{mat}_2(X_t, R_t \odot H_{t-1}; \theta_h)) \\ H_t &= (1 - Z_t) \odot H_{t-1} + Z_t \odot \tilde{H}_t \end{aligned}$$

where  $R_t$  is the reset gate, and  $Z_t$  is the interpolation factor.

## Appendix B. Graph Convolution as Matrix Operation

In this section, we demonstrate how Graph Convolutional Network (GCN) (Kipf and Welling, 2016) - a model that leverages spectral graph theory to efficiently apply convolution operator on graph can be seen as a special case of our matrix feed-forward nets.

To begin, we will reuse the graph notation  $\mathcal{G} = (\mathcal{V}, \mathcal{E})$  from Sec. 3.  $A$  is still the adjacency matrix of  $\mathcal{G}$ .  $D \in \mathbb{R}^{|\mathcal{V}| \times |\mathcal{V}|}$  be the diagonal *degree matrix* satisfied that  $D_{i,i} = \sum_j A_{i,j}$ . A normalized graph Laplacian  $L \in \mathbb{R}^{|\mathcal{V}| \times |\mathcal{V}|}$  is defined as  $L = I - D^{-\frac{1}{2}}AD^{-\frac{1}{2}}$  in case  $A$  is symmetric and  $L = I - D^{-1}A$  in case  $A$  is asymmetric;  $I$  is the identity matrix of size  $|\mathcal{V}| \times |\mathcal{V}|$ .

In spectral graph theory, the convolution operation is defined as a product between a filter  $g$  and a graph signal  $\mathbf{x} \in \mathbb{R}^{|\mathcal{V}|}$  (here, we only assume real value for each node) over the Fourier domain:

$$g \star \mathbf{x} = U g(\Lambda) U^\top \mathbf{x} \quad (14)$$

where  $U \in \mathbb{R}^{|\mathcal{V}| \times |\mathcal{V}|}$  is the matrix of eigenvectors and  $\Lambda \in \mathbb{R}^{|\mathcal{V}| \times |\mathcal{V}|}$  is the diagonal matrix of eigenvalues in the Eigen Decomposition of  $L = U\Lambda U^\top$ . In Eq. (14),  $U^\top \mathbf{x}$  can be seen as the Fourier transform of  $\mathbf{x}$  while  $U(g(\Lambda)U^\top \mathbf{x})$  is the inverse Fourier transform of the convolutional result  $g_\theta(\Lambda)U^\top \mathbf{x}$  to the spatial domain. In fact, computing Eq. (14) directly are very expensive for large graphs which requires  $O(|\mathcal{V}|^2)$  time complexity. Therefore, (Defferrard et al., 2016) propose to replace the non-parametric function  $g(\Lambda)$  with a polynomial approximation using the truncated Chebyshev expansion of order  $K - 1$ :

$$g(\Lambda) \approx g_\theta(\Lambda) = \sum_{k=0}^{K-1} \theta_k T_k(\tilde{\Lambda}) \quad (15)$$

where the parameter  $\theta = \{\theta_0, \dots, \theta_{K-1}\} \in \mathbb{R}^K$  is a vector of Chebyshev coefficients and  $T_k(\cdot)$  is the  $k$ -order Chebyshev polynomial computed by the recursive relation  $T_k(x) = 2xT_{k-1}(x) - T_{k-2}(x)$  with  $T_0 = 1$  and  $T_1 = x$ .  $\tilde{\Lambda} = 2\Lambda/\lambda_{\max} - I_{|\mathcal{V}|}$  is the scale version of  $\Lambda$  to ensure that all the eigenvalues lie in  $[-1, 1]$  ( $\lambda_{\max}$  denotes the largest eigenvalue of  $L$ ). Substitute  $g(\Lambda)$  from Eq. (15) to Eq. (14), we have:

$$\begin{aligned} g \star \mathbf{x} &\approx U g_\theta(\tilde{\Lambda}) U^\top \mathbf{x} = U \left( \sum_{k=0}^{K-1} \theta_k T_k(\tilde{\Lambda}) \right) U^\top \mathbf{x} \\ &= \left( \sum_{k=0}^{K-1} \theta_k T_k(U \tilde{\Lambda} U^\top) \right) \mathbf{x} = \left( \sum_{k=0}^{K-1} \theta_k T_k(\tilde{L}) \right) \mathbf{x} \end{aligned} \quad (16)$$

where  $\tilde{L} = 2L/\lambda_{\max} - I$  is the scaled Laplacian matrix. In stead of computing Eq. (16) recurrently from 0 to  $K-1$ , (Kipf and Welling, 2016) suggest building a deep convolutional neural networks of  $K$  layers and limit the Chebyshev estimation at each layer to 1-order (e.g.  $K = 1$ ). The transformation at one layer of the GCNs then becomes:

$$g \star \mathbf{x} \approx \theta_0 T_0(\tilde{L}) \mathbf{x} + \theta_1 T_1(\tilde{L}) \mathbf{x} = \theta_0 \mathbf{x} + \theta_1 \tilde{L} \mathbf{x} \quad (17)$$

(Kipf and Welling, 2016) further assume that  $\lambda_{\max} \approx 2$  to avoid eigenvalues decomposition of  $L$ , which is also expensive. They believe that the neural network can adapt this change in scale during training. Eq. (17) is now equivalent to:

$$g \star \mathbf{x} \approx \theta_0 \mathbf{x} + \theta_1 (L - I) \mathbf{x} = \theta_0 \mathbf{x} - \theta_1 (D^{-\frac{1}{2}} A D^{-\frac{1}{2}}) \mathbf{x}$$

Continue setting  $\theta = \theta_0 = -\theta_1$ , they come up with:

$$g \star \mathbf{x} \approx \theta (I + D^{-\frac{1}{2}} A D^{-\frac{1}{2}}) \mathbf{x} \approx \theta (\tilde{D}^{-\frac{1}{2}} \tilde{A} \tilde{D}^{-\frac{1}{2}}) \mathbf{x} \quad (18)$$

where  $\tilde{A} = A + I$  and  $\tilde{D}_{i,i} = \sum_j \tilde{A}_{i,j}$ .  $I + D^{-\frac{1}{2}} A D^{-\frac{1}{2}} \approx \tilde{D}^{-\frac{1}{2}} \tilde{A} \tilde{D}^{-\frac{1}{2}}$  is the *renormalization trick* to ensure numerical stability.

Note that up to now, we still assume that each node is correspondent with a real value. Actually, Eq. (18) can be extended to adapt the vector representation of nodes. In this case, we can rewrite Eq. (18) as:

$$Y = (\tilde{D}^{-\frac{1}{2}} \tilde{A} \tilde{D}^{-\frac{1}{2}}) X \Theta \quad (19)$$

Apparently, Eq. (19) bears a resemblance to our mat2mat formula (see Eq. (2)). The only difference is that  $(\tilde{D}^{-\frac{1}{2}} \tilde{A} \tilde{D}^{-\frac{1}{2}})$  is not a parameter but a precomputed matrix.

## References

Dzmitry Bahdanau, Kyunghyun Cho, and Yoshua Bengio. Neural machine translation by jointly learning to align and translate. *ICLR*, 2015.

Michaël Defferrard, Xavier Bresson, and Pierre Vandergheynst. Convolutional neural networks on graphs with fast localized spectral filtering. In *Advances in Neural Information Processing Systems*, pages 3844–3852, 2016.

Junbin Gao, Yi Guo, and Zhiyong Wang. Matrix neural networks. In *International Symposium on Neural Networks*, pages 313–320. Springer, 2017.

Alex Graves and Jürgen Schmidhuber. Offline handwriting recognition with multidimensional recurrent neural networks. In *Advances in neural information processing systems*, pages 545–552, 2009.

Alex Graves, Greg Wayne, and Ivo Danihelka. Neural turing machines. *arXiv preprint arXiv:1410.5401*, 2014.

Alex Graves, Greg Wayne, Malcolm Reynolds, Tim Harley, Ivo Danihelka, Agnieszka Grabska-Barwińska, Sergio Gómez Colmenarejo, Edward Grefenstette, Tiago Ramalho, John Agapiou, et al. Hybrid computing using a neural network with dynamic external memory. *Nature*, 538(7626):471–476, 2016.

Klaus Greff, Rupesh K Srivastava, and Jürgen Schmidhuber. Highway and residual networks learn unrolled iterative estimation. *ICLR*, 2017.

Aditya Grover and Jure Leskovec. node2vec: Scalable feature learning for networks. In *Proceedings of the 22nd ACM SIGKDD international conference on Knowledge discovery and data mining*, pages 855–864. ACM, 2016.

Kaiming He, Xiangyu Zhang, Shaoqing Ren, and Jian Sun. Deep residual learning for image recognition. *CVPR*, 2016.

Sepp Hochreiter and Jürgen Schmidhuber. Long short-term memory. *Neural computation*, 9(8):1735–1780, 1997.

Gao Huang, Zhuang Liu, Kilian Q Weinberger, and Laurens van der Maaten. Densely connected convolutional networks. *CVPR*, 2017.

Zhiwu Huang and Luc Van Gool. A riemannian network for spd matrix learning. In *Thirty-First AAAI Conference on Artificial Intelligence*, 2017.

Sergey Ioffe and Christian Szegedy. Batch normalization: Accelerating deep network training by reducing internal covariate shift. *arXiv preprint arXiv:1502.03167*, 2015.

Nal Kalchbrenner, Ivo Danihelka, and Alex Graves. Grid long short-term memory. *arXiv preprint arXiv:1507.01526*, 2015.

Diederik Kingma and Jimmy Ba. Adam: A method for stochastic optimization. *arXiv preprint arXiv:1412.6980*, 2014.

Thomas N Kipf and Max Welling. Semi-supervised classification with graph convolutional networks. *arXiv preprint arXiv:1609.02907*, 2016.

Yann LeCun, Yoshua Bengio, and Geoffrey Hinton. Deep learning. *Nature*, 521(7553):436–444, 2015.

Yujia Li, Daniel Tarlow, Marc Brockschmidt, and Richard Zemel. Gated graph sequence neural networks. *ICLR*, 2016.

Tomas Mikolov, Ilya Sutskever, Kai Chen, Greg S Corrado, and Jeff Dean. Distributed representations of words and phrases and their compositionality. In *Advances in Neural Information Processing Systems*, pages 3111–3119, 2013.

Tu Dinh Nguyen, Truyen Tran, Dinh Phung, and Svetha Venkatesh. Tensor-variate restricted boltzmann machines. In *Twenty-Ninth AAAI Conference on Artificial Intelligence*, 2015.

Bryan Perozzi, Rami Al-Rfou, and Steven Skiena. Deepwalk: Online learning of social representations. In *Proceedings of the 20th ACM SIGKDD international conference on Knowledge discovery and data mining*, pages 701–710. ACM, 2014.

Trang Pham, Truyen Tran, Dinh Phung, and Svetha Venkatesh. Column networks for collective classification. *AAAI*, 2017.

Guanglei Qi, Yanfeng Sun, Junbin Gao, Yongli Hu, and Jinghua Li. Matrix variate restricted boltzmann machine. In *Neural Networks (IJCNN), 2016 International Joint Conference on*, pages 389–395. IEEE, 2016.

DE Rumerhart, GE Hinton, and RJ Williams. Learning representations by back-propagation errors. *Nature*, 323:533–536, 1986.

Adam Santoro, Sergey Bartunov, Matthew Botvinick, Daan Wierstra, and Timothy Lillicrap. Meta-learning with memory-augmented neural networks. In *International conference on machine learning*, pages 1842–1850, 2016.

Franco Scarselli, Marco Gori, Ah Chung Tsoi, Markus Hagenbuchner, and Gabriele Monfardini. The graph neural network model. *IEEE Transactions on Neural Networks*, 20(1):61–80, 2009.

Nitish Srivastava, Elman Mansimov, and Ruslan Salakhutdinov. Unsupervised learning of video representations using lstms. *arXiv preprint arXiv:1502.04681*, 2015a.

Rupesh K Srivastava, Klaus Greff, and Jürgen Schmidhuber. Training very deep networks. In *Advances in neural information processing systems*, pages 2377–2385, 2015b.

Sainbayar Sukhbaatar, Arthur Szlam, Jason Weston, and Rob Fergus. End-to-end memory networks. *NIPS*, 2015.

Ilya Sutskever, Oriol Vinyals, and Quoc VV Le. Sequence to sequence learning with neural networks. In *Advances in Neural Information Processing Systems*, pages 3104–3112, 2014.

L. van der Maaten and G. Hinton. Visualizing data using t-SNE. *Journal of Machine Learning Research*, 9(2579-2605):85, 2008.

Jason Weston, Sumit Chopra, and Antoine Bordes. Memory networks. *arXiv preprint arXiv:1410.3916*, 2014.

Xianchao Xie, Shuicheng Yan, James T Kwok, and Thomas S Huang. Matrix-variate factor analysis and its applications. *IEEE transactions on neural networks*, 19(10):1821–1826, 2008.

SHI Xingjian, Zhourong Chen, Hao Wang, Dit-Yan Yeung, Wai-Kin Wong, and Wang-chun Woo. Convolutional lstm network: A machine learning approach for precipitation nowcasting. In *Advances in Neural Information Processing Systems*, pages 802–810, 2015.

Jian Yang, David Zhang, Alejandro F Frangi, and Jing-yu Yang. Two-dimensional PCA: a new approach to appearance-based face representation and recognition. *IEEE transactions on pattern analysis and machine intelligence*, 26(1):131–137, 2004.

Jieping Ye, Ravi Janardan, and Qi Li. Two-dimensional linear discriminant analysis. In *Advances in neural information processing systems*, pages 1569–1576, 2004.